

Regular Article

Influences of pH and metal ions on the interactions of oxytetracycline onto nano-hydroxyapatite and their co-adsorption behavior in aqueous solution



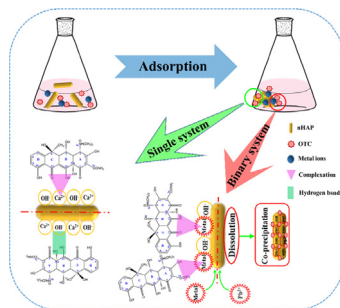
Lei Yuan^{a,1}, Ming Yan^{a,1}, Zhenzhen Huang^{a,1}, Kai He^{a,1}, Guangming Zeng^{a,*}, Anwei Chen^{b,*}, Liang Hu^c, Hui Li^a, Min Peng^a, Tiantian Huang^a, Guiqiu Chen^a

^a College of Environmental Science and Engineering, Hunan University and Key Laboratory of Environmental Biology and Pollution Control (Hunan University), Ministry of Education, Changsha 410082, PR China

^b College of Resources and Environment, Hunan Agricultural University, Changsha 410128, PR China

^c School of Minerals Processing and Bioengineering, Key Laboratory of Biohydrometallurgy of Ministry of Education, Central South University, Changsha 410083, PR China

GRAPHICAL ABSTRACT



ARTICLE INFO

Article history:

Received 21 November 2018

Revised 16 January 2019

Accepted 17 January 2019

Available online 19 January 2019

Keywords:

Oxytetracycline

Metal ions

Nano-hydroxyapatite

Ternary complexation

Adsorption mechanism

ABSTRACT

In this study, interaction of oxytetracycline (OTC) onto nano-hydroxyapatite (nHAP) was evaluated as affected by pH and metal ions. Results showed that the adsorption process of OTC was highly pH- and metallic species-dependent. The amount of sorbed OTC at four pH were in the order of pH 8.0 > pH 10.0 > pH 5.5 > pH 3.0 and reached equilibrium around 120 min, indicating adsorption affinity of four species to nHAP followed the order of $\text{OTC}^- > \text{OTC}^{2-} > \text{OTC}^\pm > \text{OTC}^+$. Adding metal ions greatly increased the distribution coefficient (K_d) of OTC between adsorbents and aqueous phases, following the order of $\text{Fe}^{3+} > \text{Cu}^{2+} > \text{Pb}^{2+} > \text{Cd}^{2+} = \text{Ca}^{2+}$ in the pH range of 3.0–10.0. Moreover, the co-adsorption behavior of OTC and heavy metals onto nHAP was also explored at pH 5.5 for the first time. OTC adsorption was significantly enhanced with the co-existence of 0.25 mmol/L Cu^{2+} or Pb^{2+} . Inversely, the presence of 0.25 mmol/L OTC slightly led to the improvement of Cu^{2+} adsorption and depression of Pb^{2+} adsorption, yet Pb^{2+} adsorption was obviously promoted with the co-existence of 0.1 mmol/L OTC. Meanwhile, adsorption of OTC and Cd^{2+} showed unapparent variation in single or binary systems. The bridging effect involving metal ions, O- and N- containing groups in OTC molecules, and $\equiv\text{CaOH}$ or $\equiv\text{POH}$ sites of nHAP resulted in the formation of ternary complexes which were responsible for the promotion of their adsorption, while dissolution-precipitation was another key mechanism with the co-existence of Pb^{2+} .

© 2019 Published by Elsevier Inc.

* Corresponding authors.

E-mail addresses: zgming@hnu.edu.cn (G. Zeng), A.Chen@hunau.edu.cn (A. Chen).

¹ These authors contribute equally to this article.

1. Introduction

Tetracycline antibiotics (TCs) are extensively applied to improve livestock growth as veterinary medicine and prevent infectious diseases in modern healthcare [1,2]. In 2011, the total usage of TCs is 9.7×10^7 kg in China, accounting for 46% of all antibiotics [3]. Due to their poor absorption and metabolism *in vivo*, TCs may be directly transmitted into environment through feces and urine as active ingredients [4,5]. To date, TCs as micro-pollutants have been found in various environmental mediums at the concentrations around 0.13–0.51 $\mu\text{g/L}$ in surface water, 86–199 $\mu\text{g/kg}$ in soils, and 4.58 mg/kg in animal dung samples [6–8]. The potential effects of TCs on organisms mainly including damage ecosystem functions and productivity, induce antibiotics resistance genes (ARGs) and increase adventure of antibiotic resistance gene transfer to human body through food chain [9–12]. Therefore, it is urgent to explore their environmental behaviors and efficient removal techniques.

Oxytetracycline (OTC) which belongs to the member of TCs, is a complicated molecule with multiple ionizable functional groups. Owing to the presence of amine groups and acid/base-active phenolic hydroxyl groups, OTC can undergo protonation-deprotonation reactions, thereby generating four species such as OTC^+ , OTC^\pm , OTC^- , and OTC^{2-} under different pH. However, these species show high persistence and good solubility in water, leading to inability to completely removal from sewage in wastewater treatment plants (WWTP) [13–17]. What's more, metal ions such as zinc and copper are frequently applied as growth promoter along with TCs in swine diets, which will induce co-contamination in the environment [18,11,19–21]. Specifically, TCs have different affinities to complex with diverse metal ions (e.g. Cu^{2+} , Ca^{2+} , Fe^{3+} , Cd^{2+} , and Pb^{2+}) to form metal ion-TCs pollutants due to the multiple N- and O-containing moieties [22–24], which may affect their environmental behaviors, including photodegradation [10,25], redox reactions [7,26], toxicity [27], and adsorption [28]. Moreover, numerous literatures have reported that it is more difficult to dislodge these co-pollutants from wastewater compared with that of single pollutant [10,29]. Although all kinds of approaches have been applied to remove heavy metals or antibiotics from water, only adsorption is considered as an effective and environment-protecting separation process for simultaneous removal of them [30,31]. Among common adsorbents such as carbon nanotube [1], clay minerals [32], bio-char [28], mesoporous silica [30], and graphene oxide [33], minerals have been frequently used as green adsorbents to treat wastewater containing heavy metals and organic pollutants due to availability, low-cost, and high-efficiency [32]. Recent studies also proved that the complexation between heavy metals and antibiotics could promote the retention of them onto minerals and soils. For example, Gu et al. reported that Cu^{2+} significantly increased the adsorption of ciprofloxacin (CIP) on goethite via forming goethite- Cu^{2+} -CIP surface complex at pH 6.0 [13]. Wang et al. found that the TC- Cu^{2+} complexes ($\text{CuH}_2\text{TC}^{2+}$, CuHTC^+ , and CuTC) had higher sorption coefficient (K_d) onto montmorillonite than their corresponding TC species (H_3TC^+ , H_2TC , and HTC^-) in the normal pH condition [34]. Further research suggested that the presence of heavy metals enhanced the adsorption of TC on soils through an ion bridging effect in the order of $\text{Cu}^{2+} > \text{Pb}^{2+} > \text{Cd}^{2+}$ at pH 3.0–10.0. Conversely, the presence of TC had little effect on the adsorption of heavy metals [23]. Although these minerals exhibited good performance in the removal of antibiotics with the maximum adsorption capacity around 20–200 mmol/kg , the adsorption of heavy metals always remained at a low level with the co-existing of antibiotics. Thus, it is necessary to seek a mineral with high adsorption capacity towards heavy metals for enhancing OTC removal.

Nano-hydroxyapatite ($\text{Ca}_{10}(\text{PO}_4)_6(\text{OH})_2$, nHAP), a universal inorganic secondary metal minerals, was widely exploited in environmental remediation, novel bone-related scaffolds, and sustained drug release systems [35]. Over the past decades, it has been used as a mature stabilizer for removing heavy metals. Metal ions (e.g. Cu^{2+} , Pb^{2+} , Cd^{2+} , Zn^{2+} , and Co^{2+}) were successfully immobilized in wastewater and contaminated soil through interaction with nHAP to form composite phosphate [36]. Owing to the reaction sites (e.g. $\equiv\text{CaOH}$, $\equiv\text{POH}$, $\equiv\text{CaOH}^{2+}$, and $\equiv\text{PO}_3\text{H}^-$) on the surface of nHAP [14], it has been gradually used to get rid of the single pollution of antibiotics in water and soil. For example, Cazalbou et al. found that the maximum sorption capacity of TC onto biomimetic apatite was 70 mmol/kg at pH 7.4 [37]. Maria Harja et al. reported that the maximum removal efficiency of OTC by uncalcined nHAP was 97.6% at pH 8.0 within 60 min when the initial concentration was 100 mmol/kg [14]. Besides, Li et al. fabricated a newly Fe-nHAP to dramatically enhance its removal efficiency for TC according to strong affinity between Fe^{3+} and OTC [38]. However, there is still a dearth of knowledge regarding whether nHAP is a promising candidate to control the combined pollution of antibiotics and heavy metals in environmental remediation. To best of our knowledge, the adsorption process of OTC in the nHAP-OTC/heavy metals binary system has not been investigated until now. Therefore, it is well worth comprehensively exploring the co-adsorption behavior of OTC and heavy metals onto nHAP.

In this work, the objectives were to investigate (1) the adsorption behavior of OTC onto nHAP at four selected pHs; (2) effect of co-existing ions on the interaction between OTC and nHAP within pH 3.0–10.0; (3) sorption of OTC and heavy metals (Cu^{2+} , Cd^{2+} , and Pb^{2+}) onto nHAP in single or binary systems; and (4) the major interaction mechanisms among OTC, heavy metals and nHAP.

2. Materials and methods

2.1. Materials

Hydrochloride salt of OTC ($\text{C}_{22}\text{H}_{24}\text{N}_2\text{O}_9\text{-HCl}$, > 95% purity) was purchased from yuanye Bio-Technology Co., Ltd (Shanghai, China). Methanol and acetonitrile were HPLC grade and obtained from Anaque Chemicals Supply (ACS, USA). Other reagents, including sodium salts, nitrates, ammonium phosphate, sodium hydroxide, and nitric acid, were all purchased from Sinopharm Chemical Reagent Co. (China). Ultrapure water (resistance = 18.25 $\text{M}\Omega/\text{cm}$) was used throughout the experiment. Antibiotic stock solution was stored in dark at 4 °C for no long than three days.

2.2. Synthesis and characterization of nHAP

The synthesis process of nHAP was based on a modified method [14,38]. Firstly, two starting solutions were prepared: dissolved the $\text{Ca}(\text{NO}_3)_2 \cdot 4\text{H}_2\text{O}$ and $(\text{NH}_4)_2\text{HPO}_4$ into the ultrapure water to achieve the solutions of 100 mmol/L Ca^{2+} and 100 mmol/L PO_4^{3-} , respectively. Under the magnetic stirring at 1000 rpm, 250 mL of 100 mmol/L Ca^{2+} was dropwise added into 150 mL of 100 mmol/L PO_4^{3-} using constant flow pump under appropriate fluid velocity for 1 h at 60 ± 1 °C. During the reaction, the pH of the suspension was monitored and adjusted to 11 ± 0.5 by NaOH solution (1 mol/L). Later, the suspension was left to mature for another 3 h at 60 ± 1 °C. Finally, the obtained precipitate was filtered through a 0.22 μm membrane, washed with ultrapure water for several times, and dried in the oven at 100 °C for 24 h.

The hydrodynamic diameter of nHAP was measured by dynamic light scattering (DLS). The morphology and composition of nHAP were obtained by a field emission scanning electron microscope equipped with an EDAX attachment (FESEM: JSM-

6700F, JEOL, Japan). The specific surface area of nHAP was determined by Brunauer-Emmett-Teller (BET) with N₂ adsorption and desorption isotherms at 77 K. The crystalline structure of nHAP was characterized by an X-ray powder diffractometer (XRD) with mono-chromated Cu K α ($\lambda = 1.5418 \text{ \AA}$) radiation. Fourier transform infrared spectra of nHAP were recorded by the KBr pellet technique using a Nicolet Nexus 670 spectrophotometer (FTIR, Japan) in range of 4000–400 cm⁻¹. X-ray photoelectron spectroscopy (XPS) analysis of nHAP was collected on an ESCALAB 250Xi spectrometer (Thermo Fisher, USA).

2.3. Adsorption experiments

Batch experiments were agitated with a speed of 160 rpm for 12 h at 25 °C, and all solutions were wrapped with foil to eliminate photodegradation [39]. The adsorbent dosage was 1 g/L. Prior to addition of nHAP, solution pH was adjusted to required value by adding negligible volumes of diluted NaOH or HCl solutions, and the final pH values were also measured. All data were recorded as the average of three duplicate experiments.

To investigate the influence of solution pH on adsorptive behaviors (kinetics and isotherms) of OTC onto nHAP, two types of adsorption experiment were carried out at pH 3.0, 5.5, 8.0, and 10.0. For kinetic experiments, 100 mg of nHAP was mixed with 100 mL OTC solution with 0.1 mmol/L of initial concentration. Time intervals of 5, 15, 30, 60, 90, 120, 150, and 180 min were selected as sampling points. For isotherm experiments, 30 mg of nHAP was added into 30 mL OTC solution with different concentrations of 0.02–0.24 mmol/L.

To reveal both co-existing ions and solution pH effects on OTC adsorption, 30 mL mixture of 0.1 mmol/L OTC with different concentrations of co-existing ions (0.25 mmol/L cations: Na⁺, Ca²⁺, Fe³⁺, Cu²⁺, Pb²⁺, and Cd²⁺; 0.5 mmol/L anions: NO₃⁻, Cl⁻, F⁻, CO₃²⁻, SO₄²⁻, and PO₄³⁻) were pre-equilibrated for 3 h at pH 3.0–10.0, and 0.1 mmol/L NaNO₃ was set to the control group. Sorption isotherms of both OTC and heavy metals (Cd²⁺, Cu²⁺, Pb²⁺) onto nHAP in single or binary systems were also studied. The mixture with pH value of 5.5 was prepared as describe above, but 30 mL mixture were contained: (1) the OTC at initial concentrations of 0.02–0.24 mmol/L with 0, 0.1 and 0.25 mmol/L heavy metals; (2) the heavy metals at initial concentrations of 0.6–2.1 mmol/L with 0, 0.1 and 0.25 mmol/L OTC. Other operations were consistent with isotherm experiment of OTC.

After adsorption, 4 mL of aliquots were taken from suspension at the set time, and quickly filtered using 0.45 μm of membrane. The aqueous OTC were determined by a high performance liquid chromatography (HPLC, Agilent 1100) on a column of Zorbax Eclipse XDB-C 18 (150 \times 4.6 nm, 5 μm) [23,40]. The aqueous heavy metals were diluted with 4 mL HNO₃ (5%) for inductively couple plasma optical emission spectroscopic analysis (ICP-OES, optima 5300 DV) [41,42]. The adsorption capacity of OTC or heavy metals (q_e , mmol/kg) and distribution coefficients of OTC (K_d , L/kg) were calculated by expressing in Eqs. (1) and (2), respectively.

$$q_e = (C_o - C_e)V/m \quad (1)$$

$$K_d = q_e/C_e \quad (2)$$

where C_o and C_e (mmol/L) are the initial and equilibrium concentrations of adsorbate, respectively; V (L) is the volume of solution and m (kg) is the mass of the adsorbent.

2.4. Spectroscopic measurements

The structure transformation of OTC arising from the complexation with metal ions was assessed by UV–vis adsorption spectra. Above all, 0.1 mmol/L OTC was mixed with an equal volume of

0.1 mmol/L metal ions (Na⁺, Ca²⁺, Fe³⁺, Cu²⁺, Pb²⁺, and Cd²⁺) under pH 3.0, 5.5, and 8.0. Then, 30 mL of mixture was pre-equilibrated for 3 h as above mentioned, the UV–vis spectra of mixture were quickly determined in the 220–500 nm range with a wavelength resolution of $\Delta\lambda = 1 \text{ nm}$.

2.5. Data analysis

In order to calculate the potential rate-controlling of the adsorption kinetics, the data were fitted with pseudo-first-order (PFO) (Eq. (3)), pseudo-second-order (PSO) (Eq. (4)), Elovich model (Eq. (5)) and intraparticle diffusion model (Eq. (6)), which are represented as follows:

$$q_t = q_e(1 - \exp(-k_1t)) \quad (3)$$

$$q_t = k_2q_e^2t/(1 + k_2q_et) \quad (4)$$

$$q_t = \ln(\alpha\beta t + 1)/\beta \quad (5)$$

$$q_t = k_{id}t^{0.5} + c \quad (6)$$

where q_t (mmol/kg) and q_e (mmol/kg) represent the adsorption capacity of adsorbent at time t (min) and equilibrium time, respectively; k_1 (1/min) and k_2 (kg/(mmol·min)) are rate constant of PFO and PSO, respectively; α (mmol/kg·min) and β (kg/mmol) are initial rate constant of chemisorption and constant of surface coverage and activation energy in Elovich equation, respectively; k_{id} (mmol/kg·min^{0.5}) is the intraparticle diffusion rate constant and c (mmol/kg) is a constant of the boundary layer thickness; t (min) is contact time.

The Langmuir (Eq. (7)) and Freundlich (Eq. (8)) models were applied to describe the equilibrium nature of OTC and heavy metals onto nHAP at different conditions, respectively. The equations are as follows:

$$q_e = q_{max}bC_e/(1 + bC_e) \quad (7)$$

$$q_e = K_fC_e^n \quad (8)$$

where q_e (mmol/kg) represents the adsorption capacity of adsorbent at equilibrium; C_e (mmol/L) is the equilibrium concentrations of adsorbate; q_{max} (mmol/kg) and b (L/mmol) are the Langmuir model adsorption parameters, where q_{max} represents the maximum sorption capacity of adsorbate onto adsorbent, and b is related to sorption affinity. K_f (mmol¹⁻ⁿLⁿ/kg) and n are the Freundlich model adsorption parameter, where K_f relates to adsorption capacity, and n is the empirical constant associated with adsorption intensity.

The Chi-square test (χ^2) and the coefficient of determination (R^2) were also used in order to further evaluate the reliability of various models, where smaller χ^2 and higher R^2 value implied a better fitting of model with the experimental data [43]. All parameters in the equation were derived from the stimulation of OriginLab 8.0 software.

3. Results and discussion

3.1. Characterization of the sorbents

The morphology and composition of nHAP were characterized by FESEM and EDAX, respectively. As seen in Fig. 1A, the FESEM image indicates that the nHAP is needle-like shape, 20–50 nm in diameter and 100–200 nm in length. Due to aggregation, the structure of nHAP shows stacked and irregular surfaces with intergranular porosity. Fig. 1B shows that the hydrodynamic diameter of nHAP in suspension is 141.8 nm after pretreating by ultrasound. The main reasons why an overestimated diameter was measured

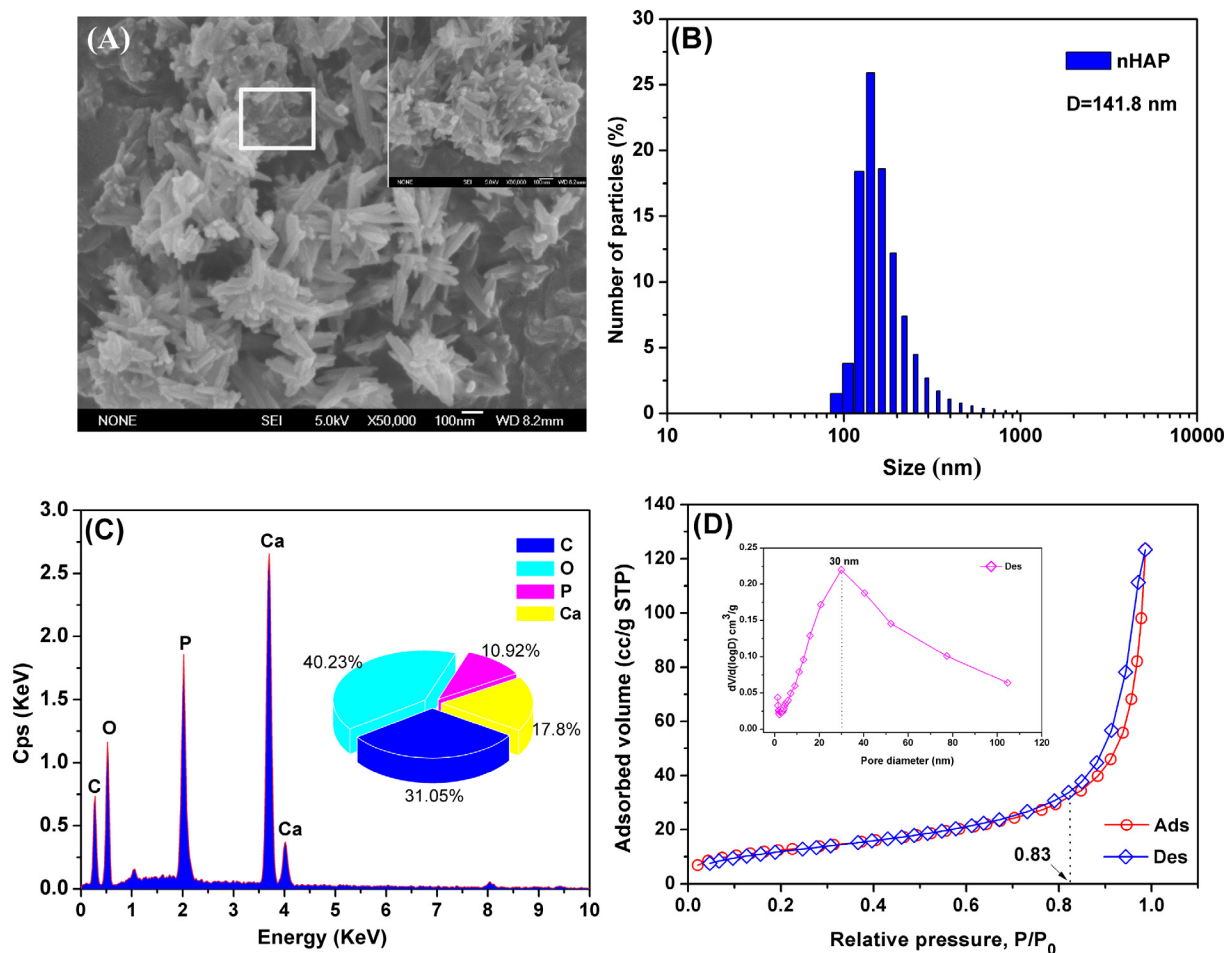


Fig. 1. Characterization of the nHAP: (A) FESEM image; (B) Hydrodynamic diameters distribution; (C) EDAX analysis of the needle-like substance in the white square on FESEM image; (D) Nitrogen sorption isotherms, and pore size distribution obtained by the desorption branch of the isotherms based on BJH model.

in DLS analysis compared with that in FESEM was that the DLS analysis was conducted with the sample in the hydrated state, while in the FESEM the estimated size was performed in the solid state [44]. The corresponding EDAX spectrum of native nHAP in Fig. 1C demonstrates that the Ca/P molar ratio is 1.63 in the presence of calcium, phosphorus and oxygen, which proves the composition of sample as hydroxyapatite. Besides, Fig. 1D displays the full N_2 adsorption-desorption isotherms and the pore distribution curve for nHAP. The BET surface area and the total pore volume of nHAP are $55.24 \text{ m}^2/\text{g}$ and $0.19 \text{ cm}^3/\text{g}$, respectively. On the basis of IUPAC classification, nHAP possesses a type IV isotherms with a hysteresis loop at approximately $P/P_0 = 0.83\text{--}0.99$, implying the characteristics of mesoporous materials [45]. The pore size distribution curve obtained by the desorption branch of the isotherms based on BJH model is also inserted in Fig. 1D. It can be seen that the size of pores are centered at 30 nm and not evenly distributed on the whole. The phase purity of nHAP was also analyzed by XRD. From Fig. 2A, the XRD diffraction peaks of nHAP are well indexed to the reference JCPDS file number (No. 09-0423) [46].

The FT-IR spectra of OTC and nHAP are presented in Fig. 2B. In the FT-IR spectrum of OTC, the broad band between 3600 cm^{-1} and 3000 cm^{-1} were attributed to the H-bonded hydroxyl groups in phenolic and alcoholic groups. The peaks at 1669 cm^{-1} and 1528 cm^{-1} belonged to the skeletal vibration of C=O at C_2 site and =NH₂ at N_{2a} site in ring A (seen in Fig. 5A). The peaks at 1615 cm^{-1} and 1582 cm^{-1} were attributed to C=O at C_{11} site in ring C and =NH at N_{4a} site in ring A, respectively, while the peak

at 1457 cm^{-1} was assigned to C=C skeletal vibration. In the FT-IR spectrum of nHAP, the characteristic band around 3567 cm^{-1} and the peak at 3446 cm^{-1} were attributed to O–H group hosted by the adsorbed water and nHAP framework, respectively [38]. The peak at 1093 cm^{-1} or 1035 cm^{-1} and the peak at 605 cm^{-1} or 565 cm^{-1} were relevant to asymmetrical stretching and bending modes of PO_4^{3-} ions, respectively. Meanwhile, the peak at 962 cm^{-1} was attributed to symmetric stretching mode of the PO_4^{3-} ions [47]. Due to the presence of HPO_4^{2-} , a small peak at 874 cm^{-1} was also detected.

3.2. Kinetics of OTC adsorption

The adsorption kinetic plotted in Fig. 3A as adsorption capacities vs contact time is nonlinear. It is noteworthy that the curves under different solution pH exhibit the similar trend. OTC adsorption onto nHAP rapidly increased within the first 15 min due to the abundant adsorption sites. After 15 min, adsorption rate slowly decreased, and gradually reached equilibrium at 120 min.

To understand the time-dependent adsorption of OTC onto nHAP, PFO, PSO, Elovich and intraparticle diffusion models were applied to fit the experiment data. The kinetic parameters are presented in Table 1. PFO and PSO are considered to determine the rate-limiting step of the adsorption process at first. Compared with PFO, the smaller χ^2 (0.96–8.00) and higher R^2 value (0.968–0.982) were found in PSO and the values of $q_{e,cal}$ simulated by PSO were more close to the $q_{e,exp}$ values, which implied that OTC sorption

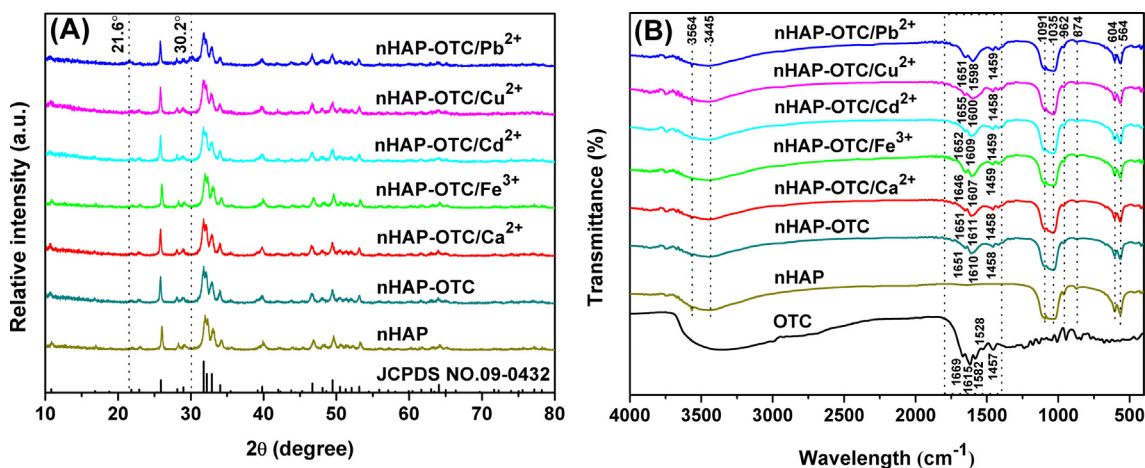


Fig. 2. XRD patterns (A) and FT-IR spectra (B) of nHAP, nHAP-OTC, nHAP-OTC/Ca²⁺, nHAP-OTC/Fe³⁺, nHAP-OTC/Cd²⁺, nHAP-OTC/Cu²⁺, and nHAP-OTC/Pb²⁺, respectively.

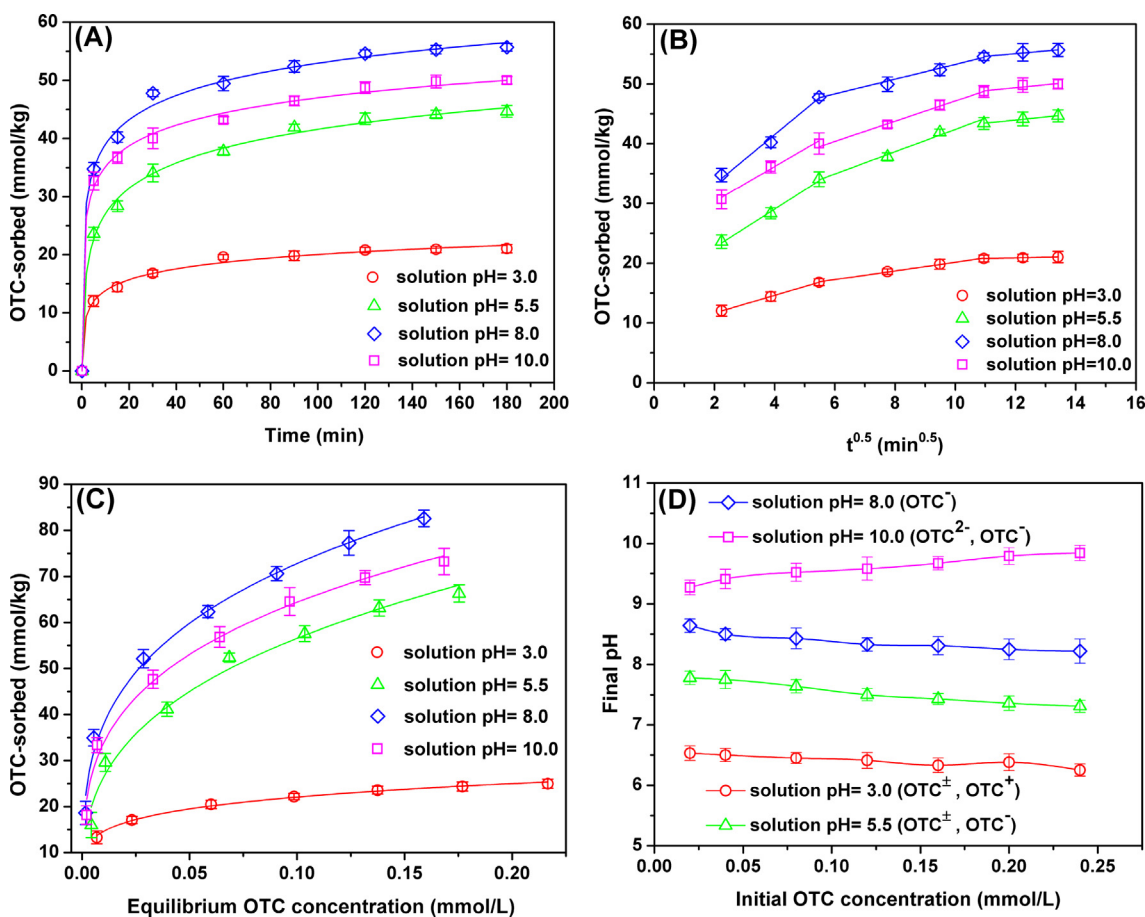


Fig. 3. (A) Adsorption kinetics of OTC on nHAP at different solution pH, the lines represent fitted curves of Elovich equation. C₀ (OTC) = 0.1 mmol/L, m/V = 1 g/L, T = 25 °C; (B) Intraparticle diffusion model for the OTC adsorption on nHAP; (C) adsorption isotherms of OTC on HAP at different solution pH, the lines represent fitted curves of Freundlich equations. m/V = 1 g/L, t = 12 h, T = 25 °C; (D) Final pH values after OTC adsorption corresponding to adsorption isotherms (mainly species show in brackets).

onto nHAP was uppermost controlled by chemisorption [48,49]. The results of PSO rate constant K_2 (kg/mmol·min) and the initial adsorption rate h ($K_2q_e^2$, mmol/kg·min), greatly impacted by the species distribution of OTC, were noted as 0.0049–0.0094 kg/mmol·min and 4.19–14.76 mmol/kg·min, respectively. The initial adsorption rates under four pH values followed an order of pH 8.0 > pH 10.0 > pH 5.5 > pH 3.0, indicating that adsorption affinity of different species followed the order as: OTC⁻ > OTC²⁻ > OTC[±] >

OTC⁺, especially at the beginning of the adsorption process [50]. However, previous studies pointed out that the idea to restrict the fit to only PFO and PSO was unsupported since the adsorption process often took place in complicated adsorbate/adsorbent systems, including often complex molecules, sometimes heterogeneous surface [37]. Therefore, Elovich model, identified as the best-fitted (highest R^2 (>0.990) and lowest χ^2 (0.23–1.03)) model, was chosen to further illustrate reaction mechanism. In combination

Table 1
Kinetic parameters of PFO, PSO, Elovich and Intraparticle diffusion models for OTC adsorption onto nHAP as effect by solution pH.

| Kinetic model | Parameter | Solution pH | | | |
|-------------------------|--|-------------|--------|--------|--------|
| | | 3.0 | 5.5 | 8.0 | 10.0 |
| | $q_{e,exp}$ (mmol/kg) | 21.04 | 44.67 | 55.70 | 50.19 |
| PFO | $q_{e,cal}$ (mmol/kg) | 19.71 | 41.30 | 51.80 | 45.55 |
| | k_1 (min^{-1}) | 0.10 | 0.16 | 0.28 | 0.22 |
| | R^2 | 0.928 | 0.911 | 0.938 | 0.918 |
| | χ^2 | 3.40 | 18.62 | 19.55 | 20.15 |
| PSO | $q_{e,cal}$ (mmol/kg) | 21.11 | 44.46 | 54.88 | 48.32 |
| | k_2 (kg/mmol·min) | 0.0094 | 0.0065 | 0.0049 | 0.0057 |
| | h (mmol/kg·min) | 4.19 | 12.85 | 14.76 | 13.31 |
| | R^2 | 0.980 | 0.970 | 0.982 | 0.968 |
| | χ^2 | 0.96 | 6.27 | 5.64 | 8.00 |
| Elovich | α (mmol/kg·min) | 43.33 | 145.42 | 389.63 | 328.57 |
| | β (kg/mmol) | 0.371 | 0.258 | 0.166 | 0.195 |
| | R^2 | 0.995 | 0.997 | 0.997 | 0.997 |
| | χ^2 | 0.23 | 0.63 | 1.03 | 0.66 |
| Intraparticle diffusion | k_{1d} (mmol/kg·min ^{0.5}) | 1.476 | 3.217 | 4.151 | 2.919 |
| | c_1 (mmol/kg) | 8.713 | 16.196 | 24.912 | 24.510 |
| | $(R_1)^2$ | 0.998 | 0.990 | 0.984 | 0.975 |
| | $(\chi_1)^2$ | 4.17 | 8.21 | 12.33 | 15.42 |
| | k_{2d} (mmol/kg·min ^{0.5}) | 0.728 | 1.861 | 1.329 | 1.694 |
| | c_2 (mmol/kg) | 12.889 | 23.786 | 40.952 | 30.21 |
| | $(R_2)^2$ | 0.997 | 0.956 | 0.992 | 0.992 |
| | $(\chi_2)^2$ | 5.99 | 21.33 | 8.94 | 7.82 |
| | k_{3d} (mmol/kg·min ^{0.5}) | 0.095 | 0.517 | 0.450 | 0.503 |
| | c_3 (mmol/kg) | 19.759 | 37.75 | 49.60 | 43.34 |
| | $(R_3)^2$ | 0.996 | 0.988 | 0.985 | 0.918 |
| | $(\chi_3)^2$ | 6.32 | 12.17 | 13.83 | 22.83 |

with the assumption of this model, we concluded that OTC molecules were primarily adsorbed onto the heterogeneous sites of nHAP via chemical action.

Since the above kinetic models were unable to describe the mass transfer steps in OTC adsorption, intraparticle diffusion model was further fitted in Fig. 3B. As seen, the plot of this model was multi-linear containing three distinct parts. The first stage (first 15 min) with the steepest segment was mainly ascribed to the transfer of OTC from liquid phase to the external surface of nHAP through film diffusion [51]. Due to the higher affinity of OTC⁻ to nHAP, the maxima of k_{1d} (mmol/kg) was obtained at pH 8.0 in Table 1. The second stage (30–120 min) showed a gradual adsorption process controlled by intraparticle diffusion (from external surface into the pores of nHAP). In addition, the intraparticle diffusion started to reach saturation at the last stage (120–180 min) because of the decrease in the active sites for nHAP. Thus, we found that both film diffusion and intraparticle diffusion existed in the diffusion process. Furthermore, all of the linear plots did not pass through the origin, which also proved that intraparticle diffusion was not the sole rate-controlling step [43].

3.3. Isotherms of OTC adsorption

Two most prevailing isotherm models (Langmuir and Freundlich) were applied to analyze the data (Fig. 3C), and relevant parameters were calculated and listed in Table 2. As shown in Table 2, Freundlich model presented higher R^2 (0.982–0.991) and smaller χ^2 (0.10–6.22) compared with Langmuir model, implying that the adsorption of OTC on nHAP was heterogeneous with multilayer uptake. Besides, the n values (0.17–0.33) defined as heterogeneity factor is much less than 1, suggesting that adsorption sites on nHAP interact with OTC via weak free energies [48].

In generally, the adsorption capacity and adsorption mechanism are influenced by solution pH through changing both the surface chemistry of adsorbents and the ionization state of pollutant. The OTC's K_f varied from 33.34 to 139.38 $\text{mmol}^{-1}\text{L}^n/\text{kg}$ (Table 2). It was obvious that K_f increased rapidly with increasing pH values

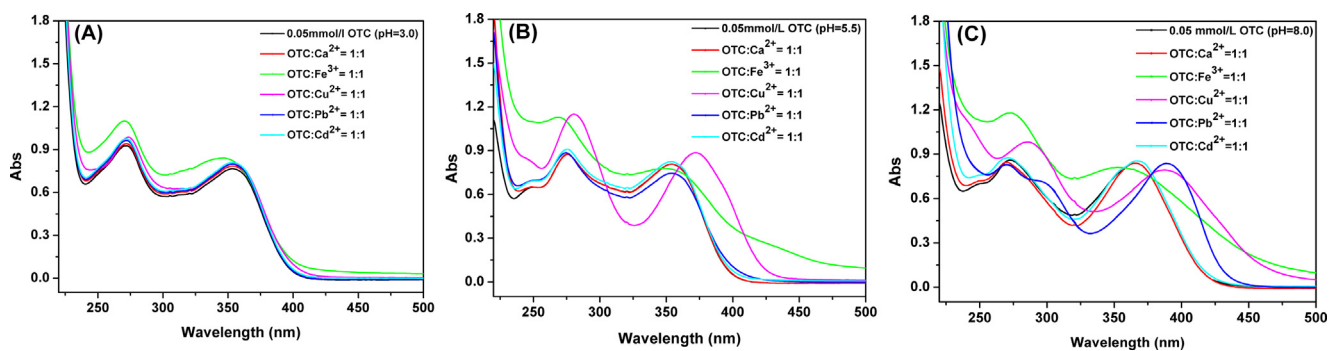
from 3.0 to 8.0, and then marginally decreased with increasing pH values from 8.0 to 10.0. The trend kept similar pace with the pH-regulated distributions of OTC⁻. However, the adsorption capacity at pH 3.0 was about 4 times smaller than that at other pH values, mainly attribution to two aspects: (1) destruction of the embedding calcium triangles structure contributed to the interaction between hydroxyl group and hydroxide ions under acidic medium [50], resulting in the depression of both hydrogen bonding and complexation between nHAP and OTC, followed by the maximum fluctuation of solution pH from 3.0 to 6.5 in Fig. 3C; (2) when solution pH was under PZC of nHAP (6.5–7.0) [14], the surface charge of nHAP was positive and the major species of OTC are OTC⁺ and OTC[±], which might produce a lasting electrostatic repulsion on reaction interface. Combined with Fig. 3C and D, no matter how solution pH was changed between 5.5 and 10.0, the adsorption capacity always floated in a small range. Thus, nHAP is an outstanding adsorbent for coping with antibiotic wastewater at various pH except for strong acidity. At pH > 7.0, the main types of OTC are OTC⁻, OTC²⁻, and OTC[±] with higher affinity to nHAP, but electrostatic repulsion is stronger than electrostatic attraction. We speculate that electrostatic forces should play a secondary role in adsorption process.

3.4. Metal ions — OTC interaction in solution

The interaction between OTC and metal ions was studied via spectroscopic measurements. UV-vis spectra and reaction mechanisms of OTC-metal complexes are shown in Fig. 4 and Table 3. As shown in Fig. 4, different degrees of spectral redshifts were observed in mixed systems due to the significant intramolecular charge transfer between OTC and metal ions [28]. Literatures have reported that TCs' A ring chromophore contributed to the adsorption band at 250–300 nm, meanwhile the BCD ring chromophore contributed to the adsorption band at both 250–300 and 340–380 nm [7,52]. It was pretty clear that the absorbance of OTC-Fe³⁺ complexes increased significantly around 250–300 nm within all pH values, but decreased slightly around 340–380 nm because

Table 2Langmuir and Freundlich parameters for the adsorption of OTC, Cu²⁺, Pb²⁺, and Cd²⁺ onto nHAP in single or binary systems.

| Samples | Solution pH | Langmuir model | | | | Freundlich model | | | |
|-----------------------------------|-------------|---------------------|--------------|-------|----------|--|-------|-------|----------|
| | | q_{max} (mmol/kg) | b (L/mmol) | R^2 | χ^2 | K_f (mmol ¹⁻ⁿ L ⁿ /kg) | n | R^2 | χ^2 |
| OTC | 3.0 | 24.52 | 35.69 | 0.902 | 1.80 | 33.34 | 0.179 | 0.990 | 0.10 |
| | 5.5 | 69.04 | 55.31 | 0.950 | 17.28 | 120.96 | 0.330 | 0.982 | 6.20 |
| | 8.0 | 78.27 | 123.32 | 0.908 | 50.09 | 139.38 | 0.282 | 0.991 | 5.15 |
| | 10.0 | 70.81 | 110.48 | 0.916 | 34.60 | 122.41 | 0.279 | 0.989 | 4.41 |
| OTC/0.10 mmol/L Cu ²⁺ | | 105.38 | 182.03 | 0.909 | 109.39 | 197.93 | 0.312 | 0.986 | 16.75 |
| OTC/0.25 mmol/L Cu ²⁺ | | 169.18 | 228.57 | 0.942 | 199.99 | 411.16 | 0.271 | 0.987 | 43.98 |
| OTC/0.10 mmol/L Pb ²⁺ | | 85.17 | 58.56 | 0.913 | 51.48 | 160.73 | 0.321 | 0.983 | 10.28 |
| OTC/0.25 mmol/L Pb ²⁺ | | 114.90 | 44.64 | 0.957 | 45.65 | 233.80 | 0.308 | 0.981 | 19.73 |
| OTC/0.10 mmol/L Cd ²⁺ | | 71.65 | 48.51 | 0.906 | 39.05 | 127.41 | 0.339 | 0.984 | 5.91 |
| OTC/0.10 mmol/L Cd ²⁺ | | 75.63 | 55.49 | 0.920 | 34.77 | 135.76 | 0.337 | 0.984 | 6.82 |
| Cu ²⁺ | | 758.51 | 17.50 | 0.989 | 93.22 | 721.84 | 0.197 | 0.913 | 410.01 |
| Cu ²⁺ /0.10 mmol/L OTC | | 813.14 | 33.07 | 0.988 | 122.02 | 804.09 | 0.165 | 0.895 | 682.32 |
| Cu ²⁺ /0.25 mmol/L OTC | | 865.89 | 65.01 | 0.998 | 20.74 | 887.87 | 0.153 | 0.912 | 912.70 |
| Pb ²⁺ | | 736.87 | 319.76 | 0.996 | 107.14 | 765.26 | 0.130 | 0.976 | 204.28 |
| Pb ²⁺ /0.10 mmol/L OTC | | 914.84 | 811.13 | 0.996 | 60.07 | 980.22 | 0.127 | 0.935 | 823.63 |
| Pb ²⁺ /0.25 mmol/L OTC | | 657.28 | 139.04 | 0.995 | 31.13 | 668.58 | 0.136 | 0.976 | 599.61 |
| Cd ²⁺ | | 433.18 | 44.62 | 0.992 | 21.82 | 419.34 | 0.114 | 0.969 | 307.02 |
| Cd ²⁺ /0.10 mmol/L OTC | | 453.18 | 45.06 | 0.991 | 25.37 | 438.37 | 0.115 | 0.959 | 116.92 |
| Cd ²⁺ /0.25 mmol/L OTC | | 445.56 | 44.74 | 0.999 | 37.96 | 432.41 | 0.126 | 0.988 | 318.65 |

**Fig. 4.** UV-vis. Spectra of OTC-metal complex at different solution pH. C_0 (OTC) = 0.05 mmol/L, V = 30 mL, t = 3 h, T = 25 °C.

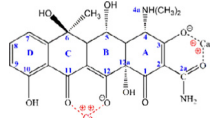
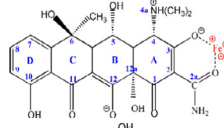
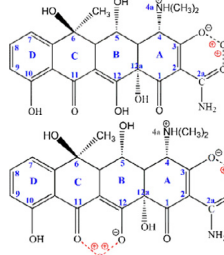
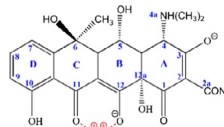
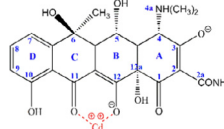
of OTC's self-degradation accelerated by Fe³⁺ [7]. Thus, Fe³⁺ likely complexes with A ring at O₃-O_{2a} site when O₃ atom becomes the first donor group, or at N_{4a}-O_{12a} site until the deprotonation of C₄ dimethylammonium group, but shows no apparent impact on BCD ring (Table 3). Significant redshifts of OTC-Cu²⁺ complexes were found around both 250–300 and 340–380 nm except pH 3.0 (seen in Fig. 4A), in which the stability constant of CuH₂OTC²⁺ was under a lower level ($\log K_{Cu,OTC} = 5.02$) at pH 3.0 so that UV-vis spectra could not detect the discernible ligand-to-metal charge transfer (LMCT). As discussed by Jezowska-Bojczuk and Jin [10,53], it could be inferred that O₃-O_{2a} site firstly bound with Cu²⁺ at low pH, with CuH₂OTC²⁺ as the unstable species. When solution pH was raised, CuHOTC⁺ or CuOTC[±] was preferentially substituted for CuH₂OTC²⁺, and chelation then converted to the O₁₁-O₁₂ site. If the ratio of copper ions to OTC was greater than 1, the O₃-O_{2a} site of CuHOTC⁺ and the N_{4a}-O_{12a} site of CuOTC[±] might further bind with free copper ions to form 1:2 ligand-to-metal complexes, with Cu₂HOTC³⁺ and Cu₂OTC²⁺ as the ultimate species, respectively. For OTC-Pb²⁺ complexes, their significant redshifts were only detected at 340–380 nm adsorption band under pH 8.0, suggesting that Pb²⁺ could only complex at the O₁₁-O₁₂ site in ring BCD, with PbOTC[±] as the unique complexes [54]. Based on Pearson's Hard-Soft-Acid-Base (HSAB) theory [55], ligands such as phenolic-diketone group and tricarbonyl group in OTC molecule would be served as soft bases owning to their large ionic radius and strong polarizability of conjugated electron clouds. Hence, Lewis acids such as Fe³⁺, Cu²⁺ and Pb²⁺ could coordinate with these soft bases in antibiotics molecules.

Although complete overlap of absorbance and peak locations occurred in both OTC-Ca²⁺ ($K_{Ca,OTC} = 10^{6.44}$) complexes and OTC-Cd²⁺ complexes ($K_{Cd,OTC} = 10^{6.9}$) due to weak iron-chelation activity, the complexes like Ca₂OTC²⁺ and CdOTC[±], were also found in previous literature [48,56,57]. For example, Ca²⁺ chelated easily with OTC²⁻ to form complexes with less protons through pH-metric titration analysis [56]. More specifically, Ca²⁺ would bond with TC to form a 1:2 ligand-to-metal complex via chelation with O₁₁-O₁₂ site resulting in the extended conformation A of TC, and then bound with OH_{12a} and N_{4a} sites through hydrogen bonding to relieve the steric crowding [57]. Just like OTC-Pb²⁺ complexes, Cd²⁺ would also complex with O₁₁-O₁₂ site of OTC²⁻ to form a unstable complex, such as CdOTC[±] [48,54].

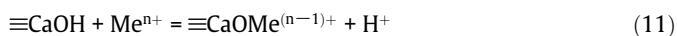
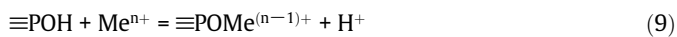
3.5. Effect of co-existing ions on OTC adsorption

The distribution coefficients (K_d , L/kg) of OTC were calculated in the presence of cations at 0.25 mmol/L or anions at 0.5 mmol/L with the solution pH values ranging from 3.0 to 10.0. The adsorption envelopes for OTC onto nHAP in the presence of co-existing ions were bell shaped in generally. As showed in Fig. 5B, the promotion in K_d influenced by the six cations had the order of Fe³⁺ > Cu²⁺ > Pb²⁺ > Cd²⁺ = Ca²⁺ = Na⁺, which was highly dependent on their complexation affinity with OTC. Xu et al. reported that the predominant surface sites in nHAP suspension were ≡POH at pH < PZC and ≡CaOH at pH > PZC, respectively, whereas ≡PO⁻ and ≡CaOH₂⁺ became significant at pH near PZC [58]. Thus, OTC could be adsorbed onto ≡CaOH₂⁺ and ≡POH mainly via cationic exchange

Table 3
Proposed reactions involving metal ions with OTC and associated constants.

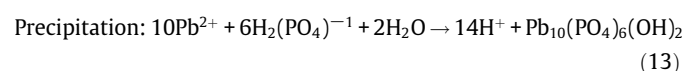
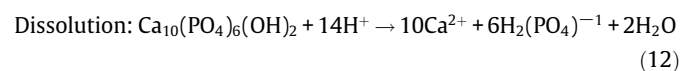
| Metal ions | Aqueous reactions | $K_{Me,OTC}$ | Proposed binding sites | Ref. |
|------------------|--|----------------------------|--|------------|
| Ca ²⁺ | $2Ca^{2+} + OTC^{2-} \rightleftharpoons Ca_2OTC^{2+}$ | $10^{6.44}$ |  | [56,57] |
| Fe ³⁺ | $Fe^{3+} + OTC \rightleftharpoons OTC-Fe^{3+}$ | $10^{9.9}$ |  | [7,52] |
| Cu ²⁺ | $Cu^{2+} + H_2OTC^{\pm} \rightleftharpoons CuH_2OTC^{2+}$ | $10^{5.02}$ |  | [10,24,53] |
| | $Cu^{2+} + HOTC^{-} \rightleftharpoons CuHOTC^{+}$ | $10^{8.19}$ | | |
| | $Cu^{2+} + CuHOTC^{+} \rightleftharpoons Cu_2HOTC^{3+}$ | $10^{4.41}$ | | |
| | $Cu^{2+} + OTC^{2-} \rightleftharpoons CuOTC^{\pm}$ $Cu^{2+} + CuOTC^{\pm} \rightleftharpoons Cu_2OTC^{2+}$ | $10^{7.86}$ $10^{4.62}$ | | |
| Pb ²⁺ | $Pb^{2+} + OTC^{2-} \rightleftharpoons PbOTC^{\pm}$ | $10^{9.17}$ |  | [54] |
| Cd ²⁺ | $Cd^{2+} + OTC^{2-} \rightleftharpoons CdOTC^{\pm}$ | $10^{6.9}$ |  | [48,54] |

with Ca²⁺ and H⁺ at pH < 7.0, and complex with ≡CaOH to form insoluble Ca₂OTC²⁺ and CaOTC[±] complexes at pH > 7.0. When Fe³⁺ or Cu²⁺ presented in the solution, K_d values were increased by two orders of magnitude at pH < 6.0, and then dropped dramatically at pH > 6.0. According to previous literatures [58,59], with the co-existence of metal ions (Meⁿ⁺ represents Fe³⁺, Cu²⁺, Cd²⁺, and Pb²⁺), the following interactions may occur:



Therefore, Meⁿ⁺ could act as a bridge ion between OTC and nHAP to form insoluble nHAP-Me-OTC ternary complexes, resulting in reinforcing the liquid-solid separation of OTC from aqueous media. The influence of metal ions on OTC adsorption might include three possible mechanisms: (1) 1:1 or 1:2 ligand-to-metal complexes had stronger affinity with nHAP than either OTC species alone; (2) at pH < 7.0, metal ions might be firstly adsorbed on surface sites via ion-exchange to form nHAP-Me while part of OTC was also loaded on the surface through weak free energies, and then the

nHAP-Me further adsorbed OTC to form stability complexes due to stronger affinity. (3) at pH > 7.0, the soluble complexes, such as Cu₂-HOTC³⁺, Cu₂OTC²⁺ and PbOTC[±], could be captured onto the negatively charged surface of nHAP via electrostatic attraction. In addition, the tendency of K_d may be greatly impacted by the solubility product constant (e.g. $K_{sp}(Fe^{3+}) = 4.0 \times 10^{-38}$; $K_{sp}(Cu^{2+}) = 4.8 \times 10^{-20}$; $K_{sp}(Pb^{2+}) = 1.0 \times 10^{-16}$), because the degree of metal precipitation is in an inverse ratio of K_{sp} value. As the pH gradually changed from acidic to alkaline, Meⁿ⁺ might gradually precipitate to form Me(OH)ⁿ⁺ in solution, so that in turn impeded the promotion effect. According to the study of Mavropoulos et al. [59], only part of Pb²⁺ (20–30%) were adsorbed on the surface by ion-exchange or complexation, and a two-stage mechanism including nHAP dissolution and hydroxypyromorphite (HP) precipitation was actually the controlling step for lead immobilization, which could be described by following interactions:



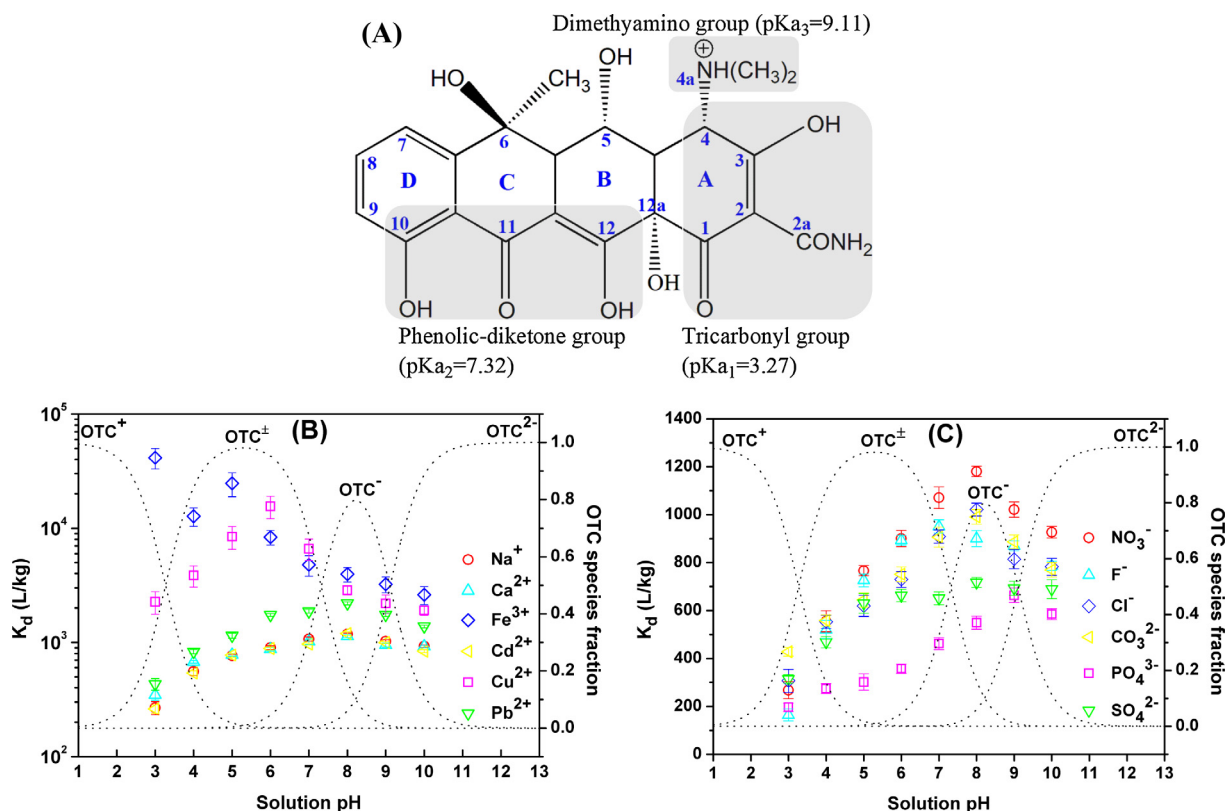


Fig. 5. (A) molecular structures and pK_a values of OTC; (B–C) Comparing the adsorbent-to-solution distribution coefficients (K_d) of OTC adsorption on nHAP with 0.25 mmol/L cations or 0.5 mmol/L anions at different solution pH, respectively (left Y axis), along with the species distribution of OTC under different pH values (right Y axis). C₀ (OTC) = 0.1 mmol/L, m/V = 1 g/L, t = 12 h, T = 25 °C.

After introduction into the reaction system, OTC molecules had more opportunities to interact with the adsorption sites during nHAP dissolution, and then the relevant complexes including Ca₂-OTC²⁺, CaOTC[±], and PbOTC[±] might be sequestered into crystal lattice during HP precipitation and re-arranged to form solid solutions. As opposed to other systems, K_d 's tendency of nHAP-OTC/Cd²⁺ remained unchanged, which might be related to the similar stability constant compared with Ca²⁺.

It is well-known that anions could not complex with OTC species. However, SO₄²⁻ and CO₃²⁻ would replace structural PO₄³⁻ to form Ca₁₀(PO₄SO₄)₆(OH)₂ and Ca₁₀(PO₄CO₃)₆(OH)₂, respectively. Meanwhile F⁻ and Cl⁻ would isomorphous substitute for structural OH⁻ to form fluorapatite (FA, Ca₁₀(PO₄)₆F₂) and chlorapatite (CA, Ca₁₀(PO₄)₆Cl₂). As shown in Fig. 5C, K_d reduction for OTC adsorption generally followed an order of PO₄³⁻ > SO₄²⁻ > CO₃²⁻ = F⁻ = Cl⁻ > NO₃⁻. This phenomenon was quite common in Hofmeister effect, both at interfaces and in solution medium [60]. In our case, the presence of PO₄³⁻ and SO₄²⁻ could significantly inhibit OTC adsorption, because PO₄³⁻ and SO₄²⁻ were easier to compete with OTC to approach superficial Ca²⁺ [50,61], and then held back the formation of nHAP-OTC binary complexes, especially compared with anion species (OTC⁻ and OTC²⁻) at pH > 7.0. In contrast, the low-affinity ligands such as CO₃²⁻, F⁻ and Cl⁻ exerted a minor inhibition to OTC adsorption. It was likely that solution pH might occupy the leading status compared with the disturbance of the three anions.

3.6. Mutual effects of OTC and heavy metal on adsorption isotherms

Up to now, little is known about the influence of heavy metal on organics adsorption, and conversely organics, to heavy metal adsorption on apatite. Therefore, nHAP was adopted as adsorbent

to illuminate their mutual effects on adsorption isotherms. Adsorption isotherms of OTC and heavy metals in single or binary systems are shown in Figs. 6 and 7, respectively. Meanwhile the corresponding parameters calculated by Langmuir and Freundlich models are also listed in Table 2. No matter in single or binary systems, the adsorption of OTC onto nHAP was Freundlich type ($R^2 > 0.98$, and $6.0 < \chi^2 < 44.0$), and the adsorption of heavy metals onto nHAP was Langmuir type ($R^2 > 0.98$, and $20.0 < \chi^2 < 125.0$). Besides, the binary systems showed different adsorption performances by means of antagonistic, neutral, and synergistic effects.

As shown in Figs. 6A and 7A, the addition of Cu²⁺ dramatically facilitated OTC adsorption on nHAP, and the presence of OTC also enhanced Cu²⁺ adsorption on nHAP with minor variation at pH 5.5, which indicated the synergistic effect on adsorption isotherms between OTC and Cu²⁺. The similar phenomenon was found on goethite, montmorillonite, and mesoporous silica [13,30,34], showing discrepancy with biochar and chitosan [28,62]. As shown in Table 2, the maximum Freundlich parameter (K_f) of OTC onto nHAP was 411.16 mmol¹⁻ⁿLⁿ/kg in the presence of Cu²⁺, which was about 3.4 times than that in single system, with K_f value of 120.96 mmol¹⁻ⁿLⁿ/kg. Conversely, the maximum sorption amount (q_{max}) of Cu²⁺ to nHAP was 865.89 mmol/kg in the presence of OTC, with an increase of 114.2% in q_{max} values compared with single system. Despite this, the n values of OTC (Freundlich fit) in binary systems were smaller than those in OTC alone system, but the b values of Cu²⁺ (Langmuir fit) in binary systems were larger than those in Cu²⁺ alone system. The above comparison revealed that the OTC-Cu²⁺ complexes (e.g. CuOTC⁰ and CuHOTC⁺) would have higher affinity to nHAP than OTC and Cu²⁺ separately.

Unlike Cu²⁺, although the addition of Pb²⁺ also considerably enhanced OTC adsorption on nHAP with K_f values ranging from 120.96 to 233.80 mmol¹⁻ⁿLⁿ/kg, opposite behaviors for Pb²⁺

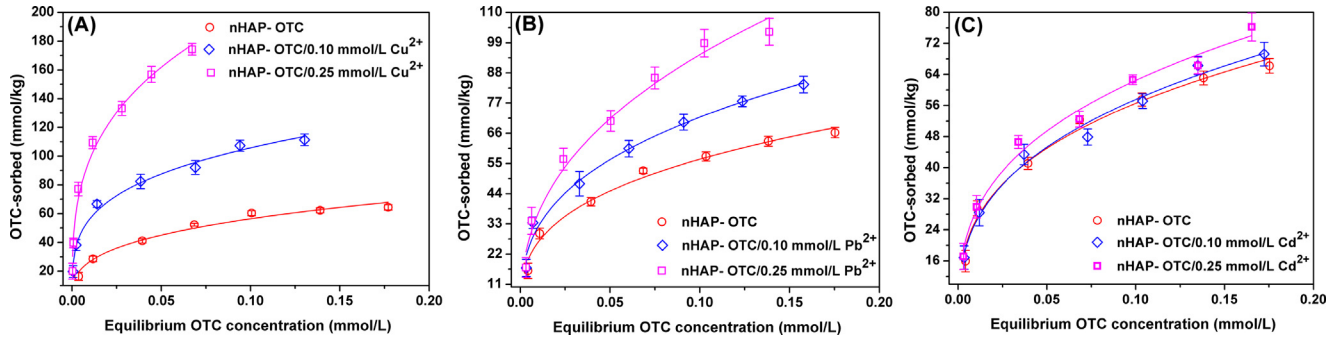


Fig. 6. Equilibrium adsorption isotherms of OTC on nHAP in single and binary systems. The lines represent fitted curves of Freundlich equations. Solution pH: 5.5, m/V = 1 g/L, t = 12 h, T = 25 °C.

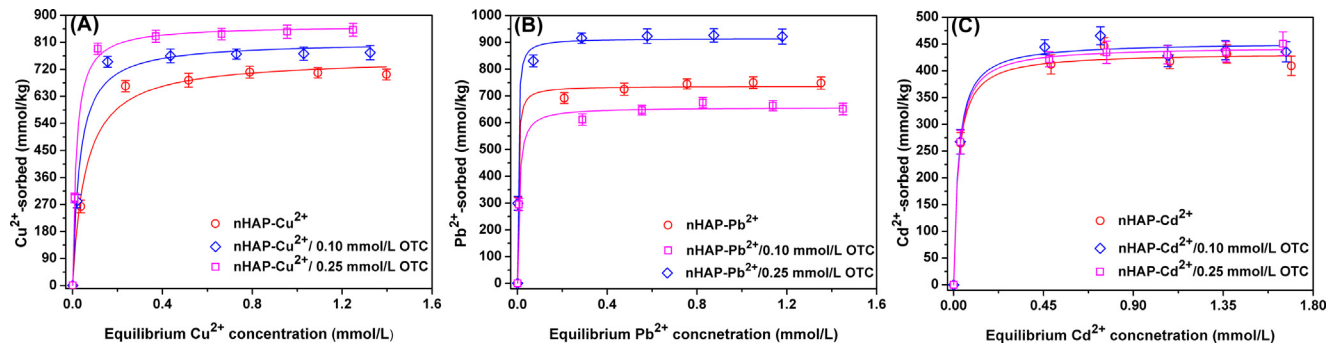


Fig. 7. Equilibrium adsorption isotherms of heavy metal on nHAP in single and binary systems. The lines represent fitted curves of Langmuir equations. Solution pH: 5.5, m/V = 1 g/L, t = 12 h, T = 25 °C.

adsorption were found in the presence of OTC, involving an increase of 28.1% at 0.10 mmol/L OTC and an decrease of 12.6% at 0.25 mmol/L OTC, respectively (Figs. 6B and 7B). Due to the special mechanism of lead immobilization by nHAP, the process was similar to co-precipitation of dissolved organic matter (DOM) and metal ions with Fe in many environments [63]. Besides, the promotion or inhibition for lead immobilization really depends on the concentration of OTC. The addition of 0.10 mmol/L OTC could complex with Pb^{2+} to form $PbOTC^0$ with higher affinity to nHAP, and the new precipitate might have larger surface area and newly formed binding sites due to OTC/ Pb^{2+} loading, implying the promotion effect on removal of both Pb^{2+} and OTC. When OTC concentration reached to 0.25 mmol/L, $\equiv POPb^{2+}$ and $\equiv CaOPb^{2+}$ on the surface were probably saturated with regard to OTC loading, and an increasing amount of OTC might blockade the metal sites due to the formation of organic multilayers, which resulted in ending the reactions of (12) and (13) at the early stage [59,63,64]. Either way, the adsorption processes of both OTC and Cd^{2+} were always independent in binary systems, which suggested the neutral effect on adsorption isotherms between OTC and Cd^{2+} (Figs. 6C and 7C).

3.7. Adsorption mechanism

XPS, FTIR and XRD analyses were performed to understand the interaction mechanism about adsorption of both OTC and metal ions onto nHAP. The results of XPS survey scans of seven samples are shown in Fig. 8A. Obviously, the major elements including Ca, P and O were found on the surfaces of these samples. The minor peaks of N 1s, Fe 2p, Cd 3d, Cu 2p and Pb 4f provided evidence of metal ion-OTC interactions on nHAP. More explanations are given below:

The Ca 2p XPS spectra are shown in Fig. 8B. Two peaks located at 350.68 and 347.11 eV were assigned to Ca $2p_{1/2}$ and Ca $2p_{3/2}$,

respectively [50]. The binding energy of Ca $2p_{3/2}$ in nHAP increased from 347.11 to 347.45 eV after OTC loading, which was attributed to the interaction between OTC and $\equiv CaOH$. When OTC and metal ions coexisted in the aqueous solution, the binding energy of Ca 2p of these samples changed slightly as compared with nHAP-OTC, since OTC exhibited higher affinity toward Fe^{3+} , Cu^{2+} and Pb^{2+} , compared with Ca^{2+} . The high resolution XPS spectra of Fe 2p and Cu 2p are also shown in Fig. 8C and D. It was obvious that the XPS spectra of Fe 2p could be divided into six peaks, including $Fe^{2+} 2p_{3/2}$ peak at 710.26 eV, $Fe^{3+} 2p_{3/2}$ peak at 712.26 eV, $Fe^{2+} 2p_{1/2}$ peak at 723.75 eV, $Fe^{3+} 2p_{1/2}$ peak at 726.54 eV, and two satellite peaks at 716.29 and 719.71 eV, indicating that Fe existed as Fe^{2+} and Fe^{3+} in the samples and coordinated with nHAP to form Fe–O bond. Besides, the peak of $Fe^{3+} 2p_{3/2}$ shifted from 712.26 eV to 713.64 eV after OTC loading because of the interaction between Fe^{3+} and OTC [30]. In the Cu 2p spectra, two peaks located at 952.70 and 932.90 eV were assigned to the Cu $2p_{1/2}$ and Cu $2p_{3/2}$, respectively [65]. The peak of Cu $2p_{3/2}$ shifted from 932.90 to 933.31 eV after OTC loading. Moreover, a new minor peak of Cu $2p_{3/2}$ was observed at 934.81 eV, which might be attributed to the interaction of Cu^{2+} with the amino groups in OTC molecules to form stable complexes [33].

As for O 1s spectra in Fig. 9, three peaks located at 532.51, 531.18 and 530.59 eV were corresponded to 16.43% of chemisorbed H_2O , 48.88% of hydroxyl groups on nHAP surface (e.g. $\equiv CaOH$ and $\equiv POH$), and 34.69% of metallic oxide as well as phosphorus oxide (M–O), respectively. When OTC was adsorbed on nHAP, the area ratio of hydroxyl groups reduced from 48.88% to 44.44% indicating that hydroxyl groups played an important role in OTC adsorption onto nHAP. Correspondingly, the increased ratio of M–O from 34.69% at 530.59 eV to 39.17% at 530.66 eV was assigned to the formation of Ca–O between $\equiv CaOH$ and OTC (Fig. 9B). Besides, the area ratio of M–O dramatically increased from

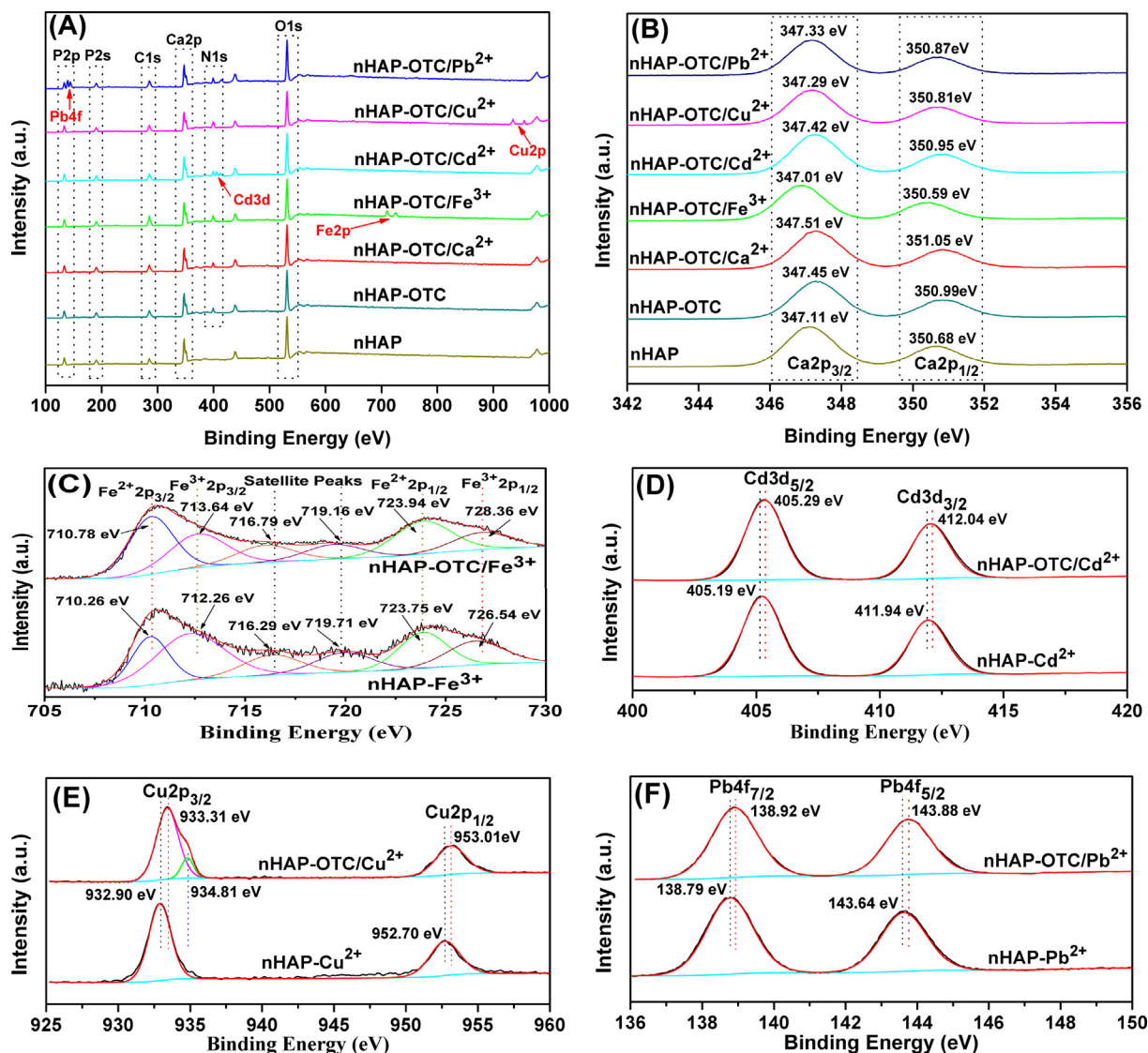


Fig. 8. XPS survey spectra (A) and the computer deconvolution Ca 2p spectra (B) of nHAP, nHAP-OTC, nHAP-OTC/Ca²⁺, nHAP-OTC/Fe³⁺, nHAP-OTC/Cd²⁺, nHAP-OTC/Cu²⁺, and nHAP-OTC/Pb²⁺. Narrow scan (C–F) of Fe 2p, Cd 3d, Cu 2p, and Pb 4f.

34.69% to 54.65%, 50.05%, and 49.63% after OTC/Fe³⁺, OTC/Cd²⁺, and OTC/Cu²⁺ loading, respectively, and the area ratio of hydroxyl groups also reduced proportionally (Fig. 9D–G). These changes might be ascribed to (1) the formation of ≡POME⁽ⁿ⁻¹⁾⁺ and ≡CaOME⁽ⁿ⁻¹⁾⁺ via the interaction shown in Eqs. (9)–(11) after metal ions loading; (2) the formation of ternary complexes, such as nHAP-Cu-OTC and nHAP-Pb-OTC, in which Cu²⁺ or Pb²⁺ could interact with O-containing groups in OTC molecules according to the proposed binding sites in Table 3.

According to FT-IR spectra (Fig. 2B), the characteristic peaks of OTC were detected in HAP-OTC spectrum at the region of 1700–1400 cm⁻¹, such as 1651, 1610 and 1458 cm⁻¹. It was likely that the peak belonged to C=O at C₂ site in ring A shifted from 1669 to 1651 cm⁻¹ due to hydrogen bonding of ≡POH and complexation with Ca²⁺ species [38]. The peak belonged to C=O at C₁₁ site in ring C became blunter and slightly shifted from 1615 to 1610 cm⁻¹ and the peak at 1582 cm⁻¹ belonging to =NH at N_{4a} site in ring A almost disappeared, which might be explained by complexation with Ca²⁺ ions on the surface of adsorbent. Compared with nHAP-OTC, the FT-IR spectra of nHAP-OTC/Cd²⁺ stayed the same after OTC/Cd²⁺ loading. While the peak located at

1669 cm⁻¹ sharply shifted to 1646 cm⁻¹ in nHAP-OTC/Fe³⁺ spectra because of the strong complexation of Fe³⁺ with O₃–O_{2a} site in OTC molecules. Moreover, the peaks of C=O groups located at 1651 and 1610 cm⁻¹ shifted to 1655 and 1600 cm⁻¹ in nHAP-OTC/Cu²⁺ spectra, respectively, testifying the chelating path of Cu₂HOTC³⁺ in Table 3. On the whole, the peak area of O–H between 3600 and 3400 cm⁻¹ dramatically decreased after the reactions, which was consistent with XPS analysis. Besides, the C=C skeletal vibration at 1457 cm⁻¹ was no lateral movement, but the peak area of this band decreased in these systems, possibly resulting from the reduction of carbon density after loading on nHAP.

Interestingly, Additional peaks (21.6° and 30.2°) were found and identified as Pb_{(10-x)Ca_x(PO₄)₆(OH)₂ in the nHAP-OTC/Pb²⁺, but the XRD patterns of other samples kept unchanged in Fig. 2A, which indicated that the reaction between OTC/Pb²⁺ and nHAP was involved into mineral interior via a mechanism of dissolution and precipitation. Although a part of nHAP could react with OTC/Pb²⁺ to produce HP-OTC deposits according to reactions of (12) and (13), nHAP-Pb-OTC might also form on the surface of nHAP via an ion bridge effect. Specifically, the peak located at 1610 cm⁻¹ shifted to 1598 cm⁻¹ in nHAP-OTC/Pb²⁺ spectra due to the complexation}

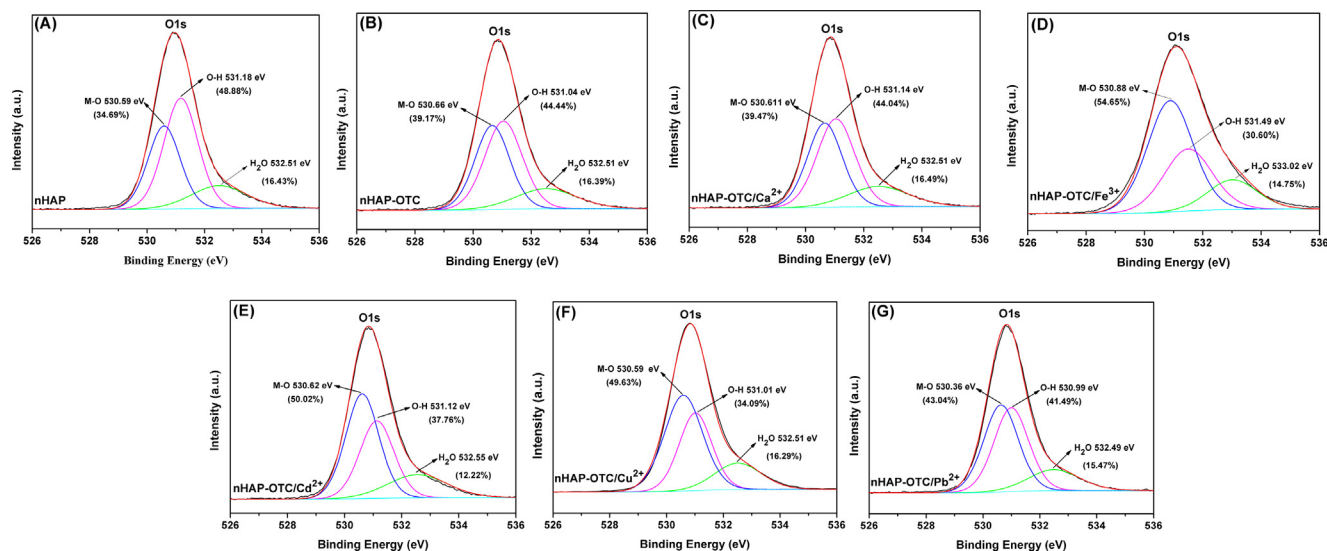


Fig. 9. (A–G) are the computer deconvolution O 1s spectra of nHAP, nHAP-OTC, nHAP-OTC/Ca²⁺, nHAP-OTC/Fe³⁺, nHAP-OTC/Cd²⁺, nHAP-OTC/Cu²⁺, and nHAP-OTC/Pb²⁺, respectively.

of Pb²⁺ with C=O at C₁₁ in OTC molecules (Fig. 2B), which could verify the possibility of OTC adsorption on nHAP-Pb. Therefore, the interaction among OTC, Pb²⁺ and nHAP was co-determined by dissolution-precipitation mechanism and bridging effects.

4. Conclusions

In summary, the interaction of OTC onto nHAP was influenced by OTC species under pH-regulation, complexing affinity of metal ions, and the process of co-precipitation in lead immobilization. The results implied that adsorptions of OTC were fitted by Elovich and Freundlich models, and adsorptions of heavy metals were described by Langmuir model. Anion species exhibited strong adsorption affinity at pH = 8.0 and high contribution to the overall adsorption of OTC. Besides, the presence of metal ions enhanced OTC adsorption via an ion bridge effect. When OTC and Cu²⁺ co-existed in the solution, the adsorption of both OTC and Cu²⁺ on nHAP were improved due to the stronger affinity of OTC-Cu²⁺ complexes compared with sole OTC or Cu²⁺. Meanwhile the interactions between Cd²⁺ and OTC were too feebler to exhibit significant changes in binary system resulting in the independent sorption of both OTC and Cd²⁺. However, the adsorption of OTC and Pb²⁺ onto nHAP was different from other systems since the interaction among OTC, Pb²⁺ and nHAP was co-determined by dissolution-precipitation mechanism and bridging effects. These findings not only help us understand how pH and metal ions influence OTC migration and transformation in the environment, but also prove the potential application of nHAP to remediate the co-contamination of them in environment.

Acknowledgements

This study was financially supported by the National Natural Science Foundation of China (51579099, 51521006 and 51879105), the Program for Changjiang Scholars and Innovative Research Team in University (IRT-13R17), and the Hunan Provincial Innovation Foundation for Postgraduate (CX2016B134).

References

[1] W.P. Xiong, Z.T. Zeng, X. Li, G.M. Zeng, R. Xiao, Z.H. Yang, Y.Y. Zhou, C. Zhang, M. Cheng, L. Hu, C.Y. Zhou, L. Qin, R. Xu, Y.R. Zhang, Multiwall-carbon

nanotube/aminomino-functionalized -53 (Fe)composites: remarkable adsorptive removal of antibiotics from aqueous solutions, *Chemosphere* 210 (2018) 1061–1069.

[2] Y. Yang, Z.T. Zeng, C. Zhang, D.L. Huang, G.M. Zeng, R. Xiao, C. Lai, C.Y. Zhou, H. Guo, W.J. Xue, M. Cheng, W.J. Wang, J.J. Wang, Construction of iodine vacancy-rich BiOI/Ag@AgI Z-scheme heterojunction photocatalysts for visible-light-driven tetracycline degradation: transformation pathways and mechanism insight, *Chem. Eng. J.* 349 (2018) 808–821.

[3] J. Li, H. Zhang, Adsorption-desorption of oxytetracycline on marine sediments: Kinetics and influencing factors, *Chemosphere* 164 (2016) 156–163.

[4] J.R. Pils, D.A. Laird, Sorption of tetracycline and chlortetracycline on K- and Ca-saturated soil clays, humic substances, and clay-humic complexes, *Environ. Sci. Technol.* 41 (2007) 1928–1933.

[5] S.J. Ye, G.M. Zeng, H.P. Wu, C. Zhang, J. Dai, J. Liang, J.F. Yu, X.Y. Ren, H. Yi, M. Cheng, C. Zhang, Biological technologies for the remediation of co-contaminated soil, *Crit. Rev. Biotechnol.* 37 (2017) 1062–1076.

[6] S.J. Ye, G.M. Zeng, H.P. Wu, C. Zhang, J. Liang, J. Dai, Z.F. Liu, W.P. Xiong, J. Wan, P. Xu, M. Cheng, Co-occurrence and interactions of pollutants, and their impacts on soil remediation-A review, *Crit. Rev. Env. Sci. Tec.* 47 (2017) 1528–1553.

[7] H. Wang, H. Yao, P. Sun, D. Li, C.H. Huang, Transformation of tetracycline antibiotics and Fe(II)/(III) species induced by their complexation, *Environ. Sci. Technol.* 50 (2015) 145–153.

[8] L. Qin, G.M. Zeng, C. Lai, D.L. Huang, P. Xu, C. Zhang, M. Cheng, X.G. Liu, S.Y. Liu, B.S. Li, H. Yi, "Gold Rush" in modern science: fabrication strategies and typical advanced applications of gold nanoparticles in sensing, *Coordin. Chem. Rev.* 359 (2018) 1–31.

[9] X.Y. Ren, G.M. Zeng, L. Tang, J.J. Wang, J. Wan, H.P. Feng, B. Song, C. Huang, X. Tang, Effect of exogenous carbonaceous materials on the bioavailability of organic pollutants and their ecological risks, *Soil Biol. Biochem.* 116 (2018) 70–81.

[10] X. Jin, S. Qiu, K. Wu, M.Y. Jia, F. Wang, C.G. Gu, A.Q. Zhang, X. Jiang, The effect of Cu²⁺ chelation on the direct photolysis of oxytetracycline: A study assisted by spectroscopy analysis and DFT calculation, *Environ. Pollut.* 214 (2016) 831–839.

[11] Z.Z. Huang, P. Xu, G.Q. Chen, G.M. Zeng, A.W. Chen, Z.X. Song, K. He, L. Yuan, H. Li, L. Hu, Silver ion-enhanced particle-specific cytotoxicity of silver nanoparticles and effect on the production of extracellular secretions of *Phanerochaete chrysosporium*, *Chemosphere* 196 (2018) 575–584.

[12] Y.R. Wang, Y. Zhu, Y. Hu, G.M. Zeng, Y. Zhang, C. Zhang, C.L. Feng, How to construct DNA hydrogels for environmental applications: advanced water treatment and environmental analysis, *Small* 14 (2018) 1–19.

[13] X.Y. Gu, Y.Y. Tan, F. Tong, C. Gu, Surface complexation modeling of coadsorption of antibiotic ciprofloxacin and Cu(II) and onto goethite surfaces, *Chem. Eng. J.* 269 (2015) 113–120.

[14] M. Harja, G. Ciobanu, Studies on adsorption of oxytetracycline from aqueous solutions onto hydroxyapatite, *Sci. Total Environ.* 628–629 (2018) 36–43.

[15] P. Xu, G.M. Zeng, D.L. Huang, C.L. Feng, S. Hu, M.H. Zhao, C. Lai, Z. Wei, C. Huang, G.X. Xie, Z.F. Liu, Use of iron oxide nanomaterials in wastewater treatment: a review, *Sci. Total Environ.* 424 (2012) 1–10.

[16] Y. Yang, C. Zhang, C. Lai, G.M. Zeng, D.L. Huang, M. Cheng, J.J. Wang, F. Chen, C. Y. Zhou, W.P. Xiong, BiOX (X = Cl, Br, I) photocatalytic nanomaterials: Applications for fuels and environmental management, *Adv. Colloid. Interfac.* 254 (2018) 77–93.

- [17] C.Y. Zhou, C. Lai, C. Zhang, G.M. Zeng, D.L. Huang, M. Cheng, L. Hu, W. Xiong, M. Chen, J.J. Wang, Y. Yang, L.B. Jiang, Semiconductor/boron nitride composites: synthesis, properties, and photocatalysis applications, *Appl. Catal. B-Environ.* 238 (2018) 6–18.
- [18] H. Wang, Y.H. Dong, Y.Y. Yang, G. Toor, X.M. Zhang, Changes in heavy metal contents in animal feeds and manures in an intensive animal production region of China, *J. Environ. Sci.* 25 (2013) 2435–2442.
- [19] Z.Z. Huang, Z.T. Zeng, A.W. Chen, G.M. Zeng, R. Xiao, P. Xu, K. He, Z.X. Song, L. Hu, M. Peng, T.T. Huang, G.Q. Chen, Differential behaviors of silver nanoparticles and silver ions towards cysteine: Bioremediation and toxicity to *Phanerochaete chrysosporium*, *Chemosphere* 203 (2018) 199–208.
- [20] L.H. Zhang, J.C. Zhang, G.M. Zeng, H.R. Dong, Y.N. Chen, C. Huang, Y. Zhu, R. Xu, Y.J. Cheng, K.J. Hou, W.C. Cao, W. Fang, Multivariate relationships between microbial communities and environmental variables during co-composting of sewage sludge and agricultural waste in the presence of PVP-AgNPs, *Bioresour. Technol.* 261 (2018) 10–18.
- [21] X. Tang, G.M. Zeng, C.Z. Fan, M. Zhou, L. Tang, J.J. Zhu, J. Wan, D.L. Huang, M. Chen, P. Xu, C. Zhang, W.P. Xiong, Chromosomal expression of CadR on *Pseudomonas aeruginosa* for the removal of Cd(II) from aqueous solutions, *Sci. Total Environ.* 636 (2018) 1355–1361.
- [22] B. Carlotti, A. Cesaretti, F. Elisei, Complexes of tetracyclines with divalent metal cations investigated by stationary and femtosecond-pulsed techniques, *Phys. Chem. Chem. Phys.* 14 (2011) 823–834.
- [23] L. Chen, J.H. Li, L.X. Chen, Colorimetric detection of mercury species based on functionalized gold nanoparticles, *ACS Appl. Mater. Inter.* 6 (2014) 15897–15904.
- [24] Y.P. Zhao, Y.Y. Tan, Y. Guo, X.Y. Gu, X.R. Wang, Y. Zhang, Interactions of tetracycline with Cd (II), Cu (II) and Pb (II) and their cosorption behavior in soils, *Environ. Pollut.* 180 (2013) 206–213.
- [25] H. Yi, D.L. Huang, L. Qin, G.M. Zeng, C. Lai, M. Cheng, S.J. Ye, B. Song, X.Y. Ren, X. Y. Guo, Selective prepared carbon nanomaterials for advanced photocatalytic application in environmental pollutant treatment and Hydrogen Production, *Appl. Catal. B-Environ.* 239 (2018) 408–424.
- [26] K. He, Z.T. Zeng, A.W. Chen, G.M. Zeng, R. Xiao, P. Xu, Z.Z. Huang, J.B. Shi, L. Hu, G.Q. Chen, Advancement of Ag-graphene based nanocomposites: An overview on synthesis and its applications, *Small* 14 (2018) 1–13.
- [27] Y. Zhang, X.Y. Cai, X.M. Lang, X.L. Qiao, X.H. Li, J.W. Chen, Insights into aquatic toxicities of the antibiotics oxytetracycline and ciprofloxacin in the presence of metal: complexation versus mixture, *Environ. Pollut.* 166 (2012) 48–56.
- [28] M.Y. Jia, F. Wang, X. Jin, Y. Song, Y.R. Bian, L.A. Boughner, X.L. Yang, C.G. Gu, X. Jiang, Q.G. Zhao, Metal ion-oxytetracycline interactions on maize straw biochar pyrolyzed at different temperatures, *Chem. Eng. J.* 304 (2016) 934–940.
- [29] A.W. Chen, C. Shang, J.H. Shao, Y.Q. Lin, S. Luo, J.C. Zhang, H.L. Huang, M. Lei, Q. R. Zeng, Carbon disulfide-modified magnetic ion-imprinted chitosan-Fe(III): A novel adsorbent for simultaneous removal of tetracycline and cadmium, *Carbohydr. Polym.* 155 (2017) 19–27.
- [30] Z.Y. Zhang, H.J. Liu, L.Y. Wu, H.C. Lan, J.H. Qu, Preparation of amino-Fe(III) functionalized mesoporous silica for synergistic adsorption of tetracycline and copper, *Chemosphere* 138 (2015) 625–632.
- [31] G.G. Wu, J.P. Ma, S. Li, J. Guan, B. Jiang, L.Y. Wang, J.H. Li, X.Y. Wang, L.X. Chen, Magnetic cooper-based metal organic framework as an effective and recyclable adsorbent for removal of two fluoroquinolone antibiotics from aqueous solutions, *J. Colloid Inter. Sci.* 528 (2018) 360–371.
- [32] M.K. Uddin, A review on the adsorption of heavy metals by clay minerals, with special focus on the past decade, *Chem. Eng. J.* 308 (2017) 438–462.
- [33] M.F. Li, Y.G. Liu, S.L. Liu, D. Shu, G.M. Zeng, X.J. Hu, X.F. Tan, L.H. Jiang, Z.L. Yan, X.X. Cai, Cu(II)-influenced adsorption of ciprofloxacin from aqueous solutions by magnetic graphene oxide/nitrotri-acetic acid nanocomposite: Competition and enhancement mechanisms, *Chem. Eng. J.* 319 (2017) 219–228.
- [34] Y.J. Wang, D.A. Jia, R.J. Sun, H.W. Zhu, D.M. Zhou, Adsorption and cosorption of tetracycline and copper(II) on montmorillonite as affected by solution pH, *Environ. Sci. Technol.* 42 (2008) 3254–3259.
- [35] M. Othmani, A. Aissa, C.G. Bac, F. Rachdi, M. Debbabi, Surface modification of calcium hydroxyapatite by grafting of etidronic acid, *Appl. Surf. Sci.* 274 (2013) 151–157.
- [36] D.J. Wang, L.Y. Chu, M. Paradelo, W.J. Peijnenburg, Y.J. Wang, D.M. Zhou, Transport behavior of humic acid-modified nano-hydroxyapatite in saturated packed column: Effects of Cu, ionic strength, and ionic composition, *J. Colloid Interf. Sci.* 360 (2011) 398–407.
- [37] S. Cazalbou, G. Bertrand, C. Drouet, Tetracycline-loaded biomimetic apatite: an adsorption study, *J. Phys. Chem. B* 119 (2015) 3014–3024.
- [38] Y.M. Li, S.G. Wang, Y. Zhang, R.M. Han, W. Wei, Enhanced tetracycline adsorption onto hydroxyapatite by Fe(III) incorporation, *J. Mol. Liq.* 247 (2017) 171–181.
- [39] R.A. Figueroa, A.A. Mackay, Sorption of oxytetracycline to iron oxides and iron oxide-rich soils, *Environ. Sci. Technol.* 39 (2005) 6664–6671.
- [40] Z.Z. Huang, G.Q. Chen, G.M. Zeng, Z. Guo, K. He, L. Hu, J. Wu, L.H. Zhang, Y. Zhu, Z.X. Song, Toxicity mechanisms and synergies of silver nanoparticles in 2,4-dichlorophenol degradation by *Phanerochaete chrysosporium*, *J. Hazard. Mater.* 321 (2016) 37–46.
- [41] L. Hu, J. Wan, G.M. Zeng, A.W. Chen, G.Q. Chen, Z.Z. Huang, K. He, M. Cheng, C.Y. Zhou, W.P. Xiong, C. Lai, P. Xu, Comprehensive evaluation of the cytotoxicity of CdSe/ZnS quantum dots in *Phanerochaete chrysosporium* by cellular uptake and oxidative stress, *Environ. Sci. Nano* 4 (2017) 2018–2029.
- [42] Z.Z. Huang, G.Q. Chen, G.M. Zeng, A.W. Chen, Y.N. Zuo, Q. Tian, Z.X. Song, Q.Y. Niu, Polyvinyl alcohol-immobilized *Phanerochaete chrysosporium*, and its application in the bioremediation of composite-polluted wastewater, *J. Hazard. Mater.* 289 (2015).
- [43] N. Tang, C.G. Niu, X.T. Li, C. Liang, H. Guo, L.S. Lin, C.W. Zheng, G.M. Zeng, Efficient removal of Cd²⁺ and Pb²⁺ from aqueous solution with amino- and thiol-functionalized activated carbon: Isotherm and kinetics modeling, *Sci. Total Environ.* 635 (2018) 1331–1344.
- [44] P.C. Lombardo, A.L. Poli, L.F. Castro, J.R. Perussi, C.C. Schmit, Photochemical deposition of silver nanoparticles on clays and exploring their antibacterial activity, *ACS Appl. Mater. Inter.* 8 (1944) 21640–21647.
- [45] L. El Hammari, H. Merroun, H.T. Coradin, S. Cassaignon, A. Laghzeil, A. Saoiabi, Mesoporous hydroxyapatites prepared in ethanol–water media: Structure and surface properties, *Mater. Chem. Phys.* 104 (2007) 448–453.
- [46] Z.Z. Zhang, M.Y. Li, W. Chen, S.Z. Zhu, N.N. Liu, L.Y. Zhu, Immobilization of lead and cadmium from aqueous solution and contaminated sediment using nano-hydroxyapatite, *Environ. Pollut.* 158 (2010) 514–519.
- [47] H. Nishida, M. Kimata, T. Ogata, T. Kawei, Malodors adsorption behavior of metal cation incorporated hydroxyapatite, *J. Environ. Chem. Eng.* 5 (2017) 2815–2819.
- [48] M.Y. Jia, F. Wang, Y.R. Bian, X. Jin, Y. Song, F.O. Kengara, R.K. Xu, X. Jiang, Effects of pH and metal ions on oxytetracycline sorption to maize-straw-derived biochar, *Bioresour. Technol.* 136 (2013) 87–93.
- [49] W. Zhang, F.H. Wang, P.L. Wang, L. Lin, Y. Zhao, P. Zou, M.J. Zhao, H. Chen, Y. Liu, Y.S. Zhang, Facile synthesis of hydroxyapatite/yeast biomass composites and their adsorption behaviors for lead (II), *J. Colloid Inter. Sci.* 477 (2016) 181–190.
- [50] L. Chen, K.S. Zhang, J.Y. He, W.H. Xu, X.J. Huang, J.H. Liu, Enhanced fluoride removal from water by sulfate-doped hydroxyapatite hierarchical hollow microspheres, *Chem. Eng. J.* 285 (2016) 616–624.
- [51] X.Q. Cai, J.H. Li, Z. Zhang, F.F. Yang, R.C. Dong, L.X. Chen, Novel Pb²⁺ ion imprinted polymers based on ionic interaction via synergy of dual functional monomers for selective solid-phase extraction of Pb²⁺ in water samples, *ACS Appl. Mater. Inter.* 6 (2014) 305–313.
- [52] H. Wang, H. Yao, P. Sun, C.H. Huang, Oxidation of tetracycline antibiotics induced by Fe(III) ions without light irradiation, *Chemosphere* 119 (2015) 1255–1261.
- [53] M. Jezowska-bojczuk, L. Lambs, H. Kozłowski, G. Berthon, Metal ion-tetracycline interactions in biological fluids. 10. Structural investigations on copper(II) complexes of tetracycline, oxytetracycline, chlortetracycline, 4-(dedimethylamino)tetracycline, and 6-deoxy-6-demethyltetracycline and discussion of their binding modes, *Inorg. Chem.* 32 (1993) 428–437.
- [54] M.A. Ghandou, H.A. Azab, A. Hassan, A.M. Ali, Potentiometric studies on the complexes of tetracycline (TC) and oxytetracycline (OTC) with some metal ions, *Monatsh. Chem.* 123 (1992) 51–58.
- [55] Z. Yang, S.Y. Jia, T.T. Zhang, N. Zhuo, Y.Y. Dong, W.B. Yang, Y.P. Yang, How heavy metals impact on flocculation of combined pollution of heavy metals-antibiotics: A comparative study, *Sep. Purif. Technol.* 149 (2015) 398–406.
- [56] M. Novák-Pékli, E.H. Mesbah, G. Pethó, Equilibrium studies on tetracycline-metal ion systems, *J. Pharmaceut. Biomed.* 14 (1996) 1025–1029.
- [57] J.M. Wessels, W.E. Ford, W. Szymczak, S. Schneider, The complexation of tetracycline and anhydrotetracycline with Mg²⁺ and Ca²⁺: a spectroscopic study, *J. Phys. Chem. B* 102 (1998) 9323–9331.
- [58] Y. Xu, F.W. Schwartz, S.Y. Traina, Sorption of Zn²⁺ and Cd²⁺ on hydroxyapatite surfaces, *Environ. Sci. Technol.* 28 (1994) 1472–1480.
- [59] E. Mavropoulos, A.M. Rossi, A.M. Costa, C.A. Perez, J.C. Moreira, M. Saldanha, Studies on the mechanisms of lead immobilization by hydroxyapatite, *Environ. Sci. Technol.* 36 (2002) 1625–1629.
- [60] P.L. Nostro, V. Mazzini, B.W. Ninham, M. Ambrosi, L.G. Dei, P. Baglioni, Specific anion effect on the kinetics of iodination of acetone, *ChemPhysChem* 17 (2016) 2567–2571.
- [61] P.S. Pinto, T.P. Medeiros, J.D. Ardisson, R.M. Lago, Role of [FeO_x(OH)_y] surface sites on the adsorption of β-lactamic antibiotics on Al₂O₃ supported Fe oxide, *J. Hazard. Mater.* 317 (2016) 327–334.
- [62] J. Kang, H. Liu, Y.M. Zheng, J.P. Chen, Systematic study of synergistic and antagonistic effects on adsorption of tetracycline and copper onto a chitosan, *J. Colloid Inter. Sci.* 344 (2010) 117–125.
- [63] C. Chen, J.J. Dynes, J. Wang, D.L. Sparks, Properties of Fe-organic matter associations via coprecipitation versus adsorption, *Environ. Sci. Technol.* 48 (2014) 13751–13759.
- [64] R. Yang, Z.W. Li, B. Huang, N.L. Luo, M. Huang, J.J. Wen, Q. Zhang, X.Q. Zhai, G.M. Zeng, Effects of Fe(III)-fulvic acid on Cu removal via adsorption versus coprecipitation, *Chemosphere* 197 (2018) 291–298.
- [65] B.Y. Huang, Y.G. Liu, B. Li, S.B. Liu, G.M. Zeng, Z.W. Zeng, X.H. Wang, Q.M. Ning, B.H. Zheng, C.P. Yang, Effect of Cu(II) ions on the enhancement of tetracycline adsorption by Fe₃O₄@SiO₂-Chitosan/graphene oxide nanocomposite, *Carbohydr. Polym.* 157 (2017) 576–585.